

# Formation of Carbon Nanostructures in Nuclear Graphite under High-Temperature In situ Electron-Irradiation

Steve Johns<sup>1</sup>, Tyler Poulsen<sup>1</sup>, Joshua J. Kane<sup>2</sup>, William E. Windes<sup>2</sup>, Rick Ubie<sup>1</sup> and Chinnathambi Karthik<sup>1,\*</sup>

<sup>1</sup>Micron School of Materials Science and Engineering, Boise State University, Boise, ID 83725, USA

<sup>2</sup>Idaho National Laboratory, 2525 Fremont Ave, Idaho Falls, ID 83402, USA

## Abstract

Defect evolution in nuclear graphite has been studied in real time using high-temperature in situ transmission electron microscopy. In situ electron-irradiation was conducted at 800°C on a 200 kV transmission electron microscope with a dose rate, given in terms of displacements per atom per second, of approximately  $1.46 \times 10^{-3}$  dpa/s. Defect domains consisting of ordered arrangements of pentagons, hexagons, and heptagons exist intrinsically in nuclear graphite and in addition are readily produced via electron-irradiation; however, at elevated temperatures these defect domains undergo atomic rearrangements resulting in the formation of carbon nanostructures via curling and closure of the basal planes. The formation of fullerenes and other structures due to thermal annealing or high-temperature electron-irradiation has been observed in disordered regions of the microstructure and interstitially between basal planes. These defect structures result in localized swelling and expansion of crystallites along the c axis; thus, it is proposed as one of the many atomic mechanisms involved in the dimensional change of nuclear graphite subjected to high-temperature irradiation.

\*Corresponding author. Tel: +1 208 426 4646. E-mail: [karthikchinnathambi@boisestate.edu](mailto:karthikchinnathambi@boisestate.edu)

## 1. Introduction

Nuclear graphite is commonly used as a moderating material as well as a key structural component in nuclear reactor designs. It is also a candidate material for the future Generation IV reactors such as the very high temperature nuclear reactor (VHTR), which may operate at up to 1000°C [1]. While in reactors, irradiation damage is accumulated in graphite over time from a fluence of fast neutrons. During irradiation, significant structural changes to the crystalline structure of graphite occurs, leading to plastic deformation. Irradiation-induced microstructural changes can play an important role in adversely affecting the mechanical properties (and hence performance) of nuclear graphites; however, a clear consensus on the various atomic mechanisms responsible for irradiation-induced microstructural evolution has not yet emerged, which yields uncertainty in accurately predicting component in-service lifetimes. In part, this uncertainty is due to the difficulty in monitoring the dynamic response of graphite during irradiation at the atomic level.

While in situ monitoring of the atomic level response of graphite in nuclear reactors remains impossible; in situ transmission electron microscopy (TEM) offers a way to monitor the dynamic atomic response of graphite during irradiation-induced defect production, in which electrons are used as a substitute for neutrons. While electron-irradiation does provide a method to overcome difficulties in monitoring the atomic level response of graphite, considerations must be taken as the dose rate for electron-irradiation ( $10^{-4}$  -  $10^{-3}$  dpa/s) is far greater than that of typical neutron-irradiation ( $10^{-7}$  dpa/s) [1]. Electron-irradiation is generally observed experimentally to primarily cause point defects; however, theory proposed by Oen [2] suggests that secondary cascade collisions have only a small contribution at high electron accelerating voltages; whereas cascade damage can be significant under irradiation by neutrons given their larger mass. In any event, the mobility and annealing rate of defects are Arrhenius in nature [3]; therefore, as the operating temperature of many nuclear reactors is above 450°C, as will be that of the VHTR, cascade damage is partially annealed out between individual cascade events, giving a net effect of isolated point-defect damage [4]. In addition, given a low density of collision cascades due to the wide spacing of graphite's basal planes [4], high-temperature neutron-irradiation may arguably be comparable to high dose-rate electron-irradiation [5,6].

On the atomic scale, radiation displacement of carbon atoms causes contraction in the a/b direction (i.e., parallel to the basal planes) and expansion in the c- direction (i.e., perpendicular to

the basal planes) [7-10]. The formation of interstitial loops between basal planes is generally believed to result in c-axis expansion due to the formation of additional basal planes and a-axis contraction from displacement of atoms within the basal planes [8]; however, alternative explanations for dimensional change in nuclear graphite have been proposed by recent theoretical models of basal plane defects, such as five- and seven-member rings [11,12], the buckling of basal planes, and the so called “ruck and tuck” of basal planes[13]. The buckling and distortion in  $sp^2$  bonded materials is known to occur in the presence of defect domains consisting of ordered arrangements of pentagons, hexagons, and heptagons, in which the atomic arrangement departs from the typical honeycomb structure [14]. Specific defects include the so called Stone-Wales defect and the Haeckelite allotrope of carbon [15]. These basal plane defects are commonly modeled two-dimensionally within graphene ribbons (isolated graphene strips). Density functional theory (DFT) and molecular dynamics (MD) studies provide a means for further analysis of the stability, scalability, and other key physical properties of materials with these defect structures. Stable basal plane defects cause strain with respect to unstressed graphene and have been proposed to result in out-of-plane “blistering” of approximately 2 Å [12]. Furthermore, MD studies have shown that graphene ribbons of a critical size (rectangular ribbons of 56 atoms or more), along with the presence of five-member rings and high temperature ( $\sim 525$ - $925^\circ\text{C}$ ), will curl and edges will meet resulting in closure and the formation of open-ended hollow structures (i.e., nanotubes) [16]. MD studies have also shown graphene-to-fullerene transformations under simulated electron-irradiation [17].

Many in situ electron-irradiation studies which analyze the c-axis expansion of crystallites, amorphization, fragmentation of basal planes, tortuous nanotexture and line-defect formation of graphite have been conducted [3,6,18-21]. Koike’s [18] room temperature electron-irradiation TEM studies showed 300% expansion along the c axis in a crystallite of highly oriented pyrolytic graphite (HOPG). The proposed mechanism for the extraordinary swelling along the c axis was given by fragmentation of basal planes due to small interstitial clusters. Room-temperature electron-irradiation studies on graphitized carbon fibers by Muto and Tanabe [19] additionally showed swelling along the c axis; however, experimental results showed homogenous swelling of the lattice spacing contradicting the proposed expansion due to fragmentation. It should also be noted that experimental results from Refs. [18] and [19] did not provide evidence of stable interstitial or vacancy dislocation loops, and their existence at room temperature remains

controversial. Other experimentally deduced mechanisms proposed for irradiation-induced structural changes in nuclear graphite at room temperature include the formation of new basal planes via dislocation climb [6]; however, electron-irradiation studies conducted at elevated temperatures remains scant [3,20,21]. Of the few studies conducted, that of Muto and Tanabe [20] showed that above temperatures of approximately 125°C the mechanisms controlling irradiation damage change at a critical dose inferred from electron diffraction patterns. At temperatures below 125°C, an increase in lattice spacing was observed; however, at temperatures above approximately 400°C lattice spacings remained unchanged, indicating that during irradiation the graphite lattice structure was not altered. As such, there remains no clear consensus to the atomic mechanisms that contribute to dimensional changes seen in nuclear graphite. While there remains a dearth of experimental studies of graphite at elevated temperatures, there have been many studies of the alterations within disordered carbonaceous species irradiated with energetic electrons, in which the formation of fullerenes, nanotubes and carbon onions have been observed [9,22-24]; however, in-situ TEM experiments of these phenomena occurring within nuclear graphites under irradiation at elevated temperatures have not yet been conducted.

Almost all graphitic precursors, such as soot particles, or any disordered graphitic species have been shown to transform to fullerene phases when subjected to sufficient irradiation with an electron beam [25]. Nuclear graphites have a complex microstructure composed of filler, binder, quinoline insoluble (QI) particles, micropores, turbostratic graphite phase, and lenticular cracks nanometers to several hundreds of nanometers in length known as Mrozowski cracks [26,27]. Mrozowski cracks form between basal planes due to weak Van der Waals bonding and volumetric shrinkage during cooling from graphitization temperatures. Given the complexity of this microstructure, a high density of various defects exists; therefore, studies conducted on areas of the microstructure with well aligned crystallites, such as filler particles, in which lattice fringes are imaged perpendicular to the c axis, may not be an accurate depiction of the bulk material. Furthermore, one might expect the presence of under-coordinated carbon atoms in poorly graphitized areas of the microstructure including phase boundaries, crystallite boundaries, and within many microstructural features such as QI particles and Mrozowski cracks. Distortions in the graphitic structure may be expected when any non-six-sided rings are present. In addition, given defect production due to high temperature and irradiation, non-equilibrium conditions are maintained while graphite is in nuclear reactors, which may stabilize fullerene phases and other

carbon nanostructures. In this work, high-temperature in situ electron-irradiation studies have been conducted on nuclear graphite IG-110. Experimental results show the morphology and ordering of carbon nanostructures not only in disordered areas of the microstructure, but interstitially between basal planes as well. The formation of these nanostructures is proposed as one of the many mechanisms resulting in the dimensional changes seen in high-temperature irradiated nuclear graphite.

## 2. Experimental

### 2.1. *Sample Preparation and Microscopy*

IG-110 nuclear graphite (Toyo Tanso Co., Kagawa, Japan) is a petroleum-coke-based, fine-grained, iso-molded nuclear graphite chosen because it is a common reference fine-grained graphite. Bulk samples of IG-110 were cut into approximately 0.5 mm thick slabs using a low-speed diamond wafering blade. Samples were further mechanically thinned to approximately 60  $\mu\text{m}$  via grinding and polishing, then specimens 3 mm in diameter were cut using a rotary disc cutter (Model 360, Southbay, San Clemente, CA). Final thinning of specimens to electron-transparency was achieved by  $\text{Ar}^+$  ion-milling using an ion polishing system (Model 691, Gatan, Pleasanton, CA). Low-voltage, low-angle ion-milling finishing was conducted on the specimens at 1 kV and  $2^\circ$  for 20 minutes after perforation to minimize ion-induced damage. In addition, electron-transparent specimens were also prepared via controlled oxidation in which the center of the 3 mm specimen discs were selectively oxidized. Experimental conditions for the preparation of TEM specimens of nuclear graphite via controlled oxidation can be found elsewhere [28]. Oxidized TEM specimens are free of irradiation-induced artifacts from ion-milling; thus, they may be used as a baseline to confirm that any experimental observations at near no irradiation damage are not artifacts caused by ion-milling induced irradiation. Bright-field and high-resolution transmission electron microscopy (HRTEM) studies were performed using a JEOL-2100 HR TEM (JEOL Ltd., Tokyo, Japan) operated at 200 kV. In-situ heating experiments were conducted with a double-tilt heating holder (Model 652, Gatan, Pleasanton, CA) in which specimens were heated at a rate of  $10^\circ\text{C}/\text{minute}$ . It should be noted that any material imaged with a TEM will experience potentially damaging electron irradiation; however, care was taken to perform all beam alignments and focusing off regions of interest to reduce electron beam-induced damage; in addition, low exposure times (0.35s) were used while imaging. Hereafter, these baseline images are labeled as having ‘near-0 dpa’.

## 2.2. DPA calculations

To evaluate the dose of radiation damage experienced by a material, a commonly used parameter that characterizes the number of atoms displaced from their normal lattice sites as a result of energetic particle bombardment is the ‘displacements per atom’ (dpa). To determine the dose experienced by a material in a transmission electron microscope, the flux of electrons at operating conditions of the microscope must first be calculated. The flux is calculated with the total beam current,  $i_{tot}$ , the radius of the beam,  $r_0$ , and the magnification used,  $M$ . The following expression represents the total flux of electrons,

$$J = \frac{i_{tot}}{C \times \pi \left(\frac{r_0}{M}\right)^2} \quad (1)$$

where  $C$  is the fundamental charge ( $1.60217662 \times 10^{-19}$  C). Evaluating the expression for a total current of  $4.01 \times 10^{-10}$  A, a beam radius of 18 mm, and a magnification of 600,000 gives a flux of  $9 \times 10^{23}$  electrons  $\text{m}^{-2}\text{s}^{-1}$ . The dose rate, given in dpa/s, is given by the product of the flux and the total cross section for atomic displacement,  $\sigma_{tot}$ .

$$\text{dpa/s} = J\sigma_{tot} \quad (2)$$

Solutions for the total cross section for atomic displacement have been provided by Oen [2] with the following two expressions:

$$\sigma_{tot}(E_i) = \frac{0.06515Z^2(E_i+0.511)^2}{E_i^2(E_i+1.022)^2} \left\{ \int_{E_D/T_m}^1 \frac{dx}{x^2} M(x, E) \right\} \quad E_D \leq T_m \leq 2E_D \quad (3)$$

$$\sigma_{tot}(E_i) = \frac{0.06515Z^2(E_i+0.511)^2}{E_i^2(E_i+1.022)^2} \left\{ \int_{E_D/T_m}^{2E_D/T_m} \frac{dx}{x^2} M(x, E) + \int_{2E_D/T_m}^1 \frac{T}{2E_D} \frac{dx}{x^2} M(x, E) \right\} \quad T_m > 2E_D \quad (4)$$

where  $E_i$  is the energy of the incident electron,  $E_D$  is the threshold energy for displacement of a given element of atomic number  $Z$ , and  $x = T/T_m$ , which is the ratio of the primary knock-on energy  $T$  and the maximum transferred energy  $T_m$  resulting from a head-on collision. The function  $M(x, E)$  yields the ratio of the Mott and Rutherford cross sections, the solutions for which are given by Ref. [29]. Assumptions implicit in Eqs. 2 – 4 follow the Kinchin and Pease Model [30] which assumes only one atomic displacement will occur for primary knock-on energies in the range  $E_D \leq T \leq 2E_D$ , and the number of atomic displacements for primary knock-on energies  $T > 2E_D$  is given by the ratio  $T/2E_D$ . Reported values for  $E_D$  in graphite show a great variation in the literature [5,9,21,31] and range from 12-60 eV; however, Banhart [9] suggests an appropriate

polycrystalline value between 15-20 eV. Assuming a value of 20 eV for  $E_D$ , and a 200 keV incident electron energy, the total displacement cross section for carbon is given in Ref. [2] as 16.25 barns. Evaluating Eq. 2 with the given values for electron flux and the total displacement cross section yields an approximated dose rate of  $1.46 \times 10^{-3}$  dpa/s.

### 3. Results and discussion

Fig. 1. shows bright-field TEM micrographs of nuclear graphite IG-110 prepared by conventional ion-milling technique. Fig.1. (a) shows a boundary region near the termination of a filler particle. Boundary regions between phases in nuclear graphite may extend several hundred nanometers and are composed of Mrozowski cracks, pores, misaligned basal planes and randomly oriented crystals. Fig.1. (b) shows QI particles that are often found in the binder phase of nuclear graphites. The micrographs shown in Fig.1. depict representative areas of the microstructure in which there is no long-range order to crystals, basal planes are misaligned, and disordered graphitic phases exist on the microscopic scale.

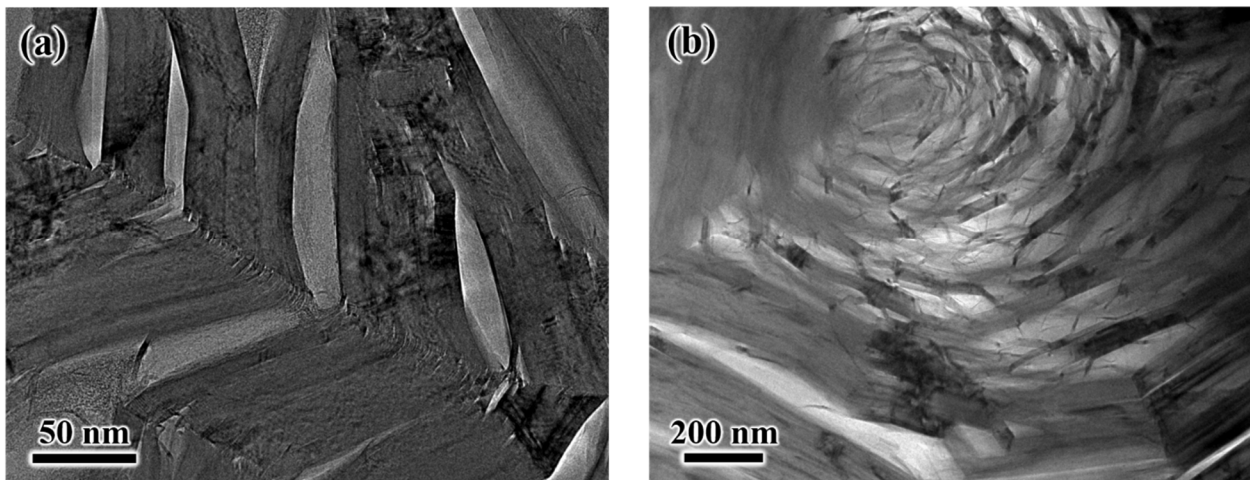


**Fig.1.** Bright-field TEM micrographs showing the complex microstructure of IG-110 in (a) a region in the phase boundary between a filler particle and the binder phase and (b) QI particles found in the binder phase.

Fig.2. (a) and (b) show a specimen of IG-110 prepared via oxidation and imaged at room temperature with very little electron beam exposure and therefore near 0 dpa. Although this technique has been shown to produce isolated artifact-free crystals of nuclear graphite [28], basal plane edges which contain under-coordinated carbon atoms are exposed (*i.e.*, while such specimens are artifact-free, they are not defect-free), whereas Fig.2. (c) and (d) show specimens of IG-110 prepared via ion-milling. The micrographs of IG-110 in Fig. 2 were all taken near 0 dpa. Fig.2. (a) was taken at room temperature while Fig. 2 (b-d) were taken at 800°C. While basal

plane edges are left largely unaltered at room temperature, curling and closure of basal plane edges is observed as loops in oxidized specimens with localized swelling indicated, Fig. 2. (b), and in ion-milled specimens as either hollow nanotube-like structures within Mrozowski cracks, Fig. 2. (c) or interstitially as a line defects, Fig. 2. (d). These results show experimentally that the curling and closure of basal planes is not a result of irradiation but of thermal annealing only. Furthermore, given Fig.2. (b), the curling and closure of basal planes cannot be explained as simply an artifact introduced by ion milling.

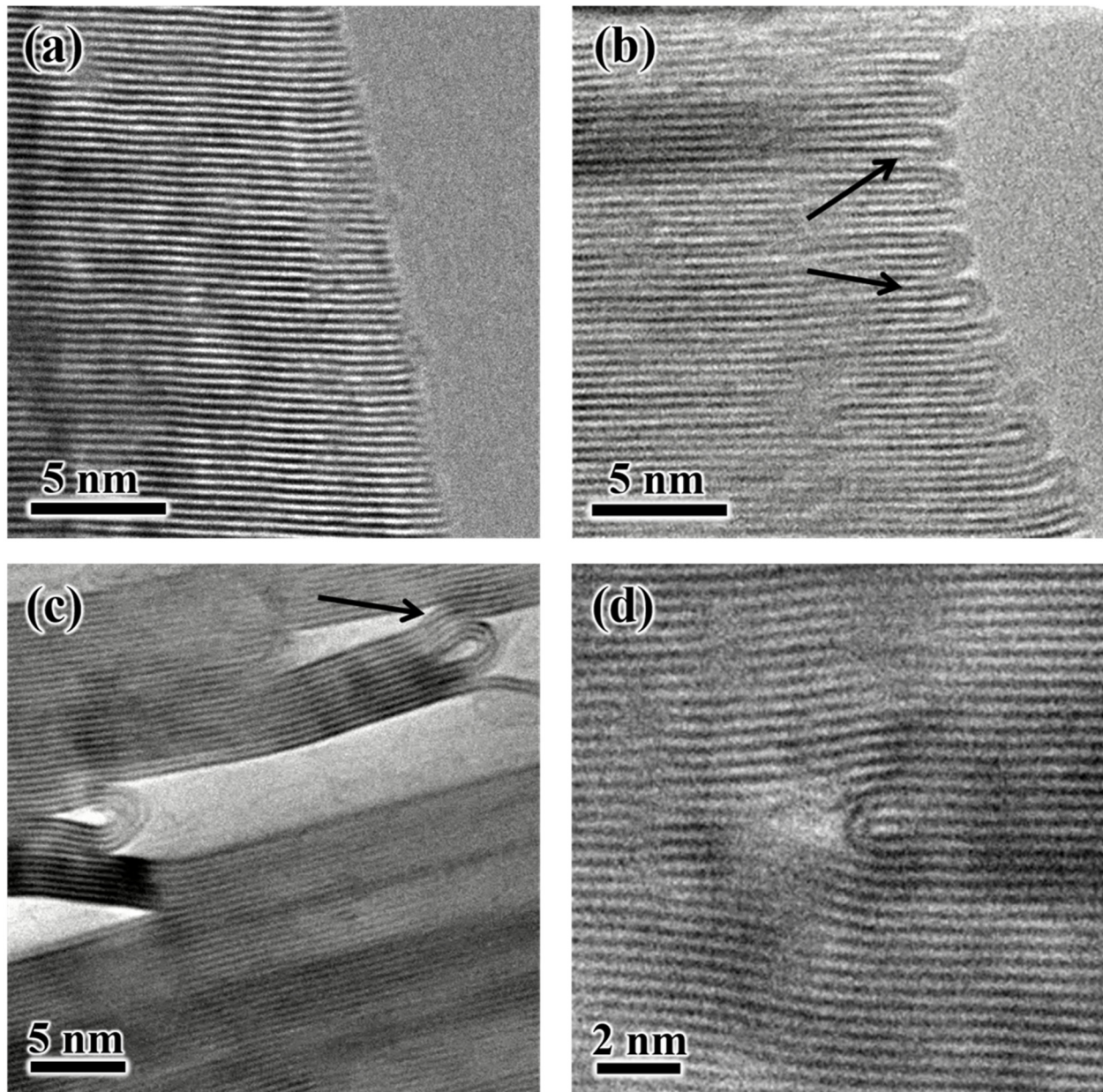


**Fig.2.** HRTEM images of IG-110 imaged at near 0 dpa. (a) TEM specimen prepared via oxidation of IG-110 imaged at room temperature showing no curling or closure of basal planes. (b)

*Oxidation-prepared TEM specimen showing curling of basal planes and localized swelling, at the edge of a crystallite imaged at 800°C. (c) Ion-milled TEM specimen imaged at 800°C showing curling and localized swelling of basal planes, indicated by an arrow, in disordered region of the microstructure. (d) Curling of incomplete basal planes around a prismatic dislocation in ion-milled IG-110 imaged at 800°C.*

Fig.3. shows the effect of electron-irradiation at 800°C on IG-110 prepared via oxidation. The oxidized specimen of IG-110 irradiated to 1.75 dpa depicted in Fig. 3 (a) shows that under-coordinated carbon atoms near the edges of crystals will transform into carbon onions upon continued irradiation.

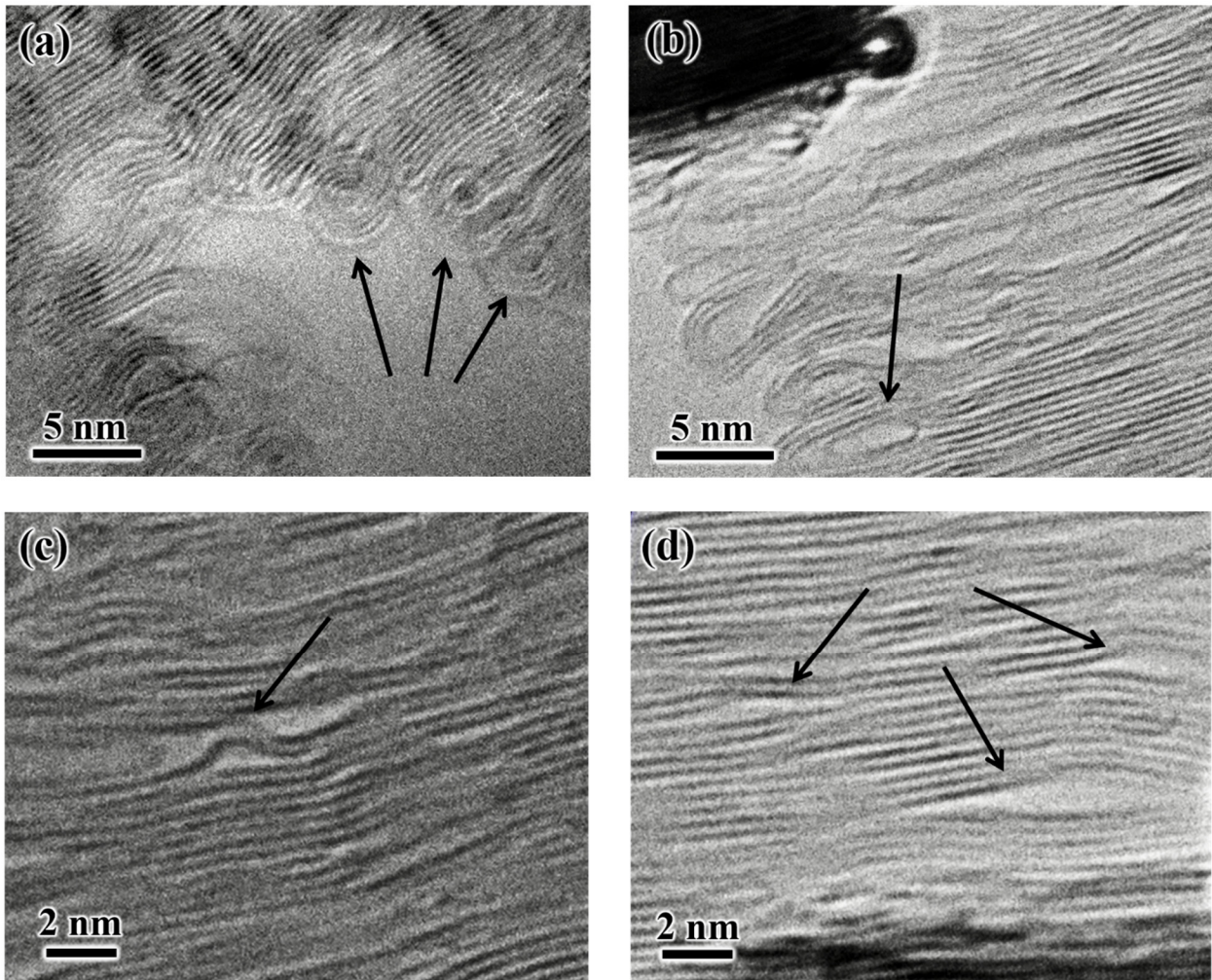


**Fig.3.** HRTEM micrographs of IG-110 prepared via oxidation imaged at 800°C. (a) Specimen irradiated to 1.75 dpa where the formation of carbon onions is indicated. (b-d) Specimen irradiated to ~1.44 dpa where significant distortion of the basal planes is observed. Area (b) shows the curling and closure of a basal plane interstitially, (c) shows the rucking of basal planes, and in (d) basal plane separation and voids are visible.

Carbon onions are a non-equilibrium structure consisting of concentric shells of fullerenes which self-assemble under irradiation. Formation of concentric-shelled fullerene phases due to electron-irradiation from graphitic or amorphous carbon precursors was first observed by Ugarte [22] and may be expected to form in any highly disordered phase of carbon irradiated at high temperatures; however, their evolution and existence in disordered phases of nuclear graphite has not previously been reported. The present experimental results shown in Fig.3. (a) show that the formation of carbon onions will occur in nuclear graphite where basal plane edges and under-coordinated atoms are exposed. As carbon onions form in un-constrained areas near voids or pores, their contribution to dimensional and property changes observed in nuclear graphite remains an open question; however, other distortions to the graphite lattice is seen to occur. The oxidized specimen of IG-110 irradiated to approximately 1.44 dpa depicted in Fig.3. (b-d) illustrates several mechanisms of basal plane distortion, including Fig.3. (b) the curling and closure of a basal plane interstitially forcing adjacent planes apart, Fig.3. (c) the rucking of basal planes, and Fig.3. (d) the separation of basal planes creating voids. It is clear from this image that many different mechanisms are responsible for observed dimension changes in nuclear graphite at elevated temperatures. The difficulties in acquiring quality micrographs (*i.e.*, snapshots) from in situ heating studies should be noted. Significant mechanical drift in all axial directions may occur during in situ analysis and increases with temperature. An in situ video showing the formation of the carbon onions is provided as Video 1 from which the snap shot shown in Fig. 3(a) is taken.

**Video 1** *HREM in situ video of nuclear graphite IG-110 prepared to electron transparency via oxidation. Specimen irradiated from approximately 0-1.75 dpa with an 200kV electron beam showing the formation of carbon onions. The video was rendered at 4 times normal speed.*

Fig.4. (a-f) shows an in situ electron-irradiation study of IG-110 prepared via ion-milling conducted at 800°C from approximately 0 to 1.77 dpa. Fig.4. (a) shows the initial state of a crystallite within the center of a QI particle, with the initial crystallite size measured along the c axis labeled. As the structure accumulates irradiation damage, displaced atoms appear to form small aggregate defects, which distort basal planes and are observed as blurred strain fields, indicated in Fig.4. (b). With continued electron-irradiation, nucleation and growth of a larger defect structure is observed in Fig.4. (c-e). Fig.4. (f) shows a nanotube-like defect interstitially formed, resulting in significant expansion in the c direction, with the width of the indicated crystallite increasing from 3.71 nm to 5.61 nm which is an increase of approximately 51%. In addition, the clear contrast of the observed defect in Fig. 4. (f) suggests that the defect must be

stable and extend through the majority of the specimen's thickness [19] (approximately 115 nm measured via electron energy loss spectroscopy with the log-ratio method [32]).

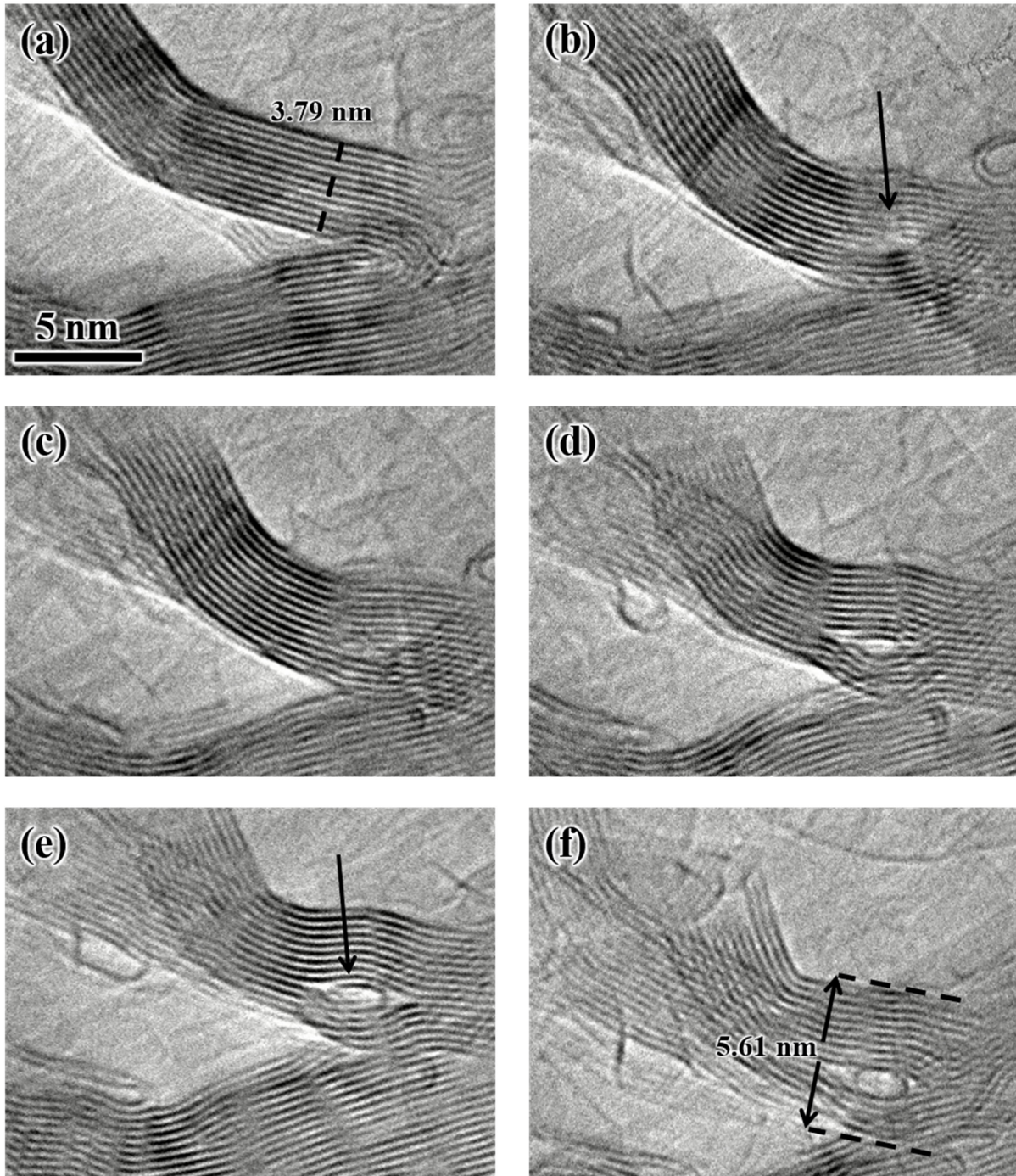


**Fig.4.** HRTEM micrographs within a QI particle at 800°C. (a) Initial micrograph at ~0 dpa with initial size of the crystallite along the *c* axis labeled. (b) After 0.90 dpa where the indicated strain field suggests the presence of defects. (c) After 1.01 dpa where accumulation of defects is apparent within the structure. (d) 1.29 dpa & (e) 1.47 dpa show the curling and closure of interstitially

displaced carbon atoms into a nanotube-like defect that remains stable under continued electron-irradiation, as shown in (f) after 1.77 dpa with final crystallite size along the  $c$  axis labeled.

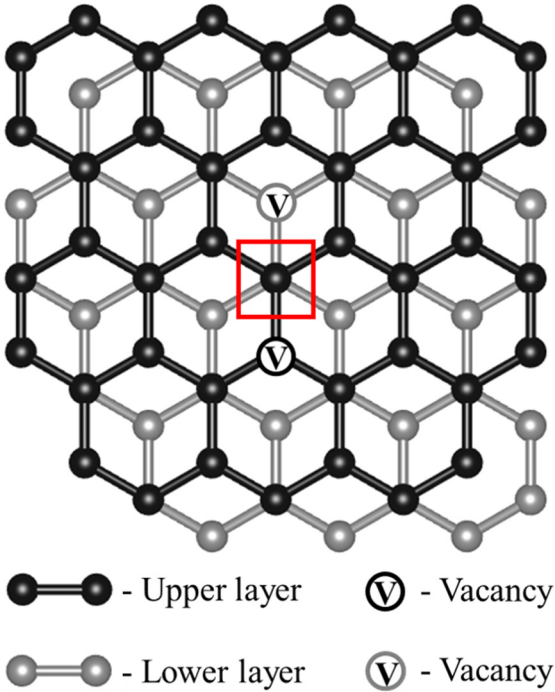


**Fig.5.** Schematic of a  $V_2^2\beta\beta$  interlayer divacancy, where the square highlights two under-coordinated atoms that may form an interlayer bond. A color version of this figure can be found online.

[35] and is depicted in Fig.5. The notation  $V_2$  denotes a vacancy species in which two atoms surrounding each vacancy are able to form bonds within the plane where two under-coordinated atoms are situated directly above one another ( $\alpha$  site), as indicated by the red square in Fig. 5. In the case of a  $V_2^2\beta\beta$  divacancy, the superscript 2 denotes the vacancies occur at second nearest interplane neighbour positions, and  $\beta$  denoting a vacant lattice site position below a ring center in the adjacent layer. This divacancy results in twofold coordinated carbon atoms which allow bonding interactions between basal planes similar to a spiro interstitial (ground state carbon atom interstitial consisting of four bonds, two bonds with each adjacent basal plane) [8]. It is proposed that the  $V_2^2\beta\beta$  interlayer divacancy will remain immobile at temperatures below 1000°C and may therefore result in further interlayer bonding from under-coordinated atoms [35]. After a  $V_2^2\beta\beta$  defect is formed, nucleation of an extended interlayer defect, such as the so called “ $V_7-V_7$  interlayer

A possible interpretation of the evolution of the hollow nanotube-like defect seen in Fig.4. (f) could be interlayer bonding occurring between basal planes. While exposed to electron-irradiation, displacement of carbon atoms from equilibrium positions occurs, resulting in interstitial and vacancy defect species. It is generally believed that, in the case of single-bonded interstitials, binding sites are created in the adjacent interlayer regions due to interruption of  $\pi$  bonding within basal planes [33], which may result in the formation of small aggregates ( $4\pm 2$  atoms) of cross-linking interstitials. Interlayer bonding may also occur from divacancy species, such as the so called  $V_2^1\beta\beta$  and  $V_2^2\beta\beta$  interlayer divacancies (in the notation of Ref. [34]); however, only the later has been proposed to result in nucleation of extended interlayer defects

defect” (in the notation of Ref. [34]) where four interlayer bonds occur as a result of two vacancy lines in adjacent layers consisting of seven vacancies in both  $\alpha$  and  $\beta$  sites along the zig-zag direction. This interlayer defect has been both simulated and found experimentally with room-temperature HRTEM studies [6,35]. It is proposed that further growth of an extended interlayer defect species may occur, and as irradiation continues, bonds in under-coordinated carbon atoms linking the basal planes are broken via atomic displacements resulting in an interstitial “ribbon of graphene” with undercoordinated carbon atoms on the edges of the ribbon. The resulting ribbon curls and closure occurs forming the nanotube-like structure (Fig.4. (f)). Further molecular dynamics studies could provide confirmation of the stability of these defect structures and a possible formation mechanism.

The mechanisms responsible for the dimension change observed in nuclear graphite while subjected to irradiation is believed to be a function of temperature. Room temperature electron-irradiation studies have proposed several mechanisms to explain the resulting dimensional change in nuclear graphite [6,18,19]. However, larger and stable defect structures have not been observed at ambient temperatures. At elevated temperatures it is generally believed that the mobility of interstitial and vacancy defects increases resulting in atomic rearrangement of atoms and/or agglomeration of point defects [8]. The curling and closure of basal planes due solely to thermal annealing, as seen in Fig. 2., has been found to occur at lower temperature (750°C, see supplementary data); however, the formation of stable fullerene defects via electron-irradiation was not achievable below 750°C in practical experimental times. The formation of the stable defect structure shown in Fig.4. (f) exemplifies the difference in the response of electron-irradiation conducted at room temperature compared to electron-irradiation at elevated temperatures. Furthermore, the experimental results of this study demonstrate that there is no single mechanism responsible for the dimensional change in nuclear graphite; thus, it is believed that many temperature-dependent mechanisms are responsible for dimensional change in nuclear graphite.

## 4. Conclusions

The formation of carbon nanostructures via curling and closure of basal planes in graphitic networks is favorable not only with increased temperature but also in the presence of under-coordinated carbon atoms and defect species. This work shows experimental evidence that under electron-irradiation conducted at 800°C, nuclear graphite will form nanostructures not only in

disordered phases of carbon, but interstitially between basal planes. The given experimental results show that the formation of carbon nanostructure defects due to thermal annealing or high-temperature electron-irradiation results in localized swelling and c-axis expansion in nuclear graphite; thus, it is an additional atomic mechanism for the observed dimensional changes in nuclear graphite subjected to high-temperature irradiation.

## Acknowledgements

The material reported here is based on work supported by the U. S. Department of Energy's EPSCoR-State/National Laboratory Partnership Program (Award # DE-SC0016427). Electron microscopy and specimen preparation was carried out at the Boise State Center for Materials Characterization (BSCMC).

## References

- [1] T.R. Allen, K. Sridharan, L. Tan, W.E. Windes, J.I. Cole, D.C. Crawford, G.S. Was, Materials Challenges for Generation IV Nuclear Energy Systems, *Nucl. Technol.* 162 (2008) 342–357, doi:10.13182/NT08-A3961.
- [2] O.S. Oen, Cross Sections for Atomic Displacements in Solids By Fast Electrons, ORNL-381, Oak Ridge National Laboratory (1965).
- [3] H.M. Freeman, A.J. Scott, R.M.D. Brydson, Thermal annealing of nuclear graphite during in-situ electron irradiation, *Carbon N. Y.* 115 (2017) 659–664, doi:10.1016/j.carbon.2017.01.057.
- [4] J.H.W. Simmons, Radiation Damage in Graphite, in: J. V. Dunworth (Ed.), 1st Edition, Pergamon, 1965.
- [5] D.F. Pedraza, J. Koike, Dimensional changes in grade H-451 nuclear graphite due to electron irradiation, *Carbon N. Y.* 32 (1994) 727–734, doi:10.1016/0008-6223(94)90095-7.
- [6] C. Karthik, J. Kane, D.P. Butt, W.E. Windes, R. Uvic, In situ transmission electron microscopy of electron-beam induced damage process in nuclear grade graphite, *J. Nucl. Mater.* 412 (2011) 321–326, doi:10.1016/j.jnucmat.2011.03.024.
- [7] R.E. Nightingale, *Nuclear Graphite*, Academic Press, (1962).
- [8] R.H. Telling, M.I. Heggie, Radiation defects in graphite, *Philos. Mag.* 87 (2007) 4797-4846, doi:10.1080/14786430701210023.

- [9] F. Banhart, Irradiation effects in carbon nanostructures, *Reports Prog. Phys.* 62 (1999) 1181–1221, doi:10.1088/0034-4885/62/8/201.
- [10] J.E. Brocklehurst, B.T. Kelly, The dimensional changes of highly-oriented pyrolytic graphite irradiated with fast neutrons at 430°C and 600°C, *Carbon N. Y.* 31 (1993) 179–183, doi:10.1016/0008-6223(93)90170-F.
- [11] F. Banhart, J. Kotakoski, A. V Krasheninnikov, Structural Defects in Graphene, *ACS Nano.* 5 (2011) 26–41, doi:10.1021/nn102598m.
- [12] M.T. Lusk, L.D. Carr, Nanoengineering defect structures on graphene, *Phys. Rev. Lett.* 100 (2008) 1–4. doi:10.1103/PhysRevLett.100.175503.
- [13] M.I. Heggie, I. Suarez-Martinez, C. Davidson, G. Haffenden, Buckle, ruck and tuck: A proposed new model for the response of graphite to neutron irradiation, *J. Nucl. Mater.* 413 (2011) 150–155, doi:10.1016/j.jnucmat.2011.04.015.
- [14] J. Gruber, A.C. Lang, J. Griggs, M.L. Taheri, G.J. Tucker, M.W. Barsoum, Evidence for Bulk Ripplations in Layered Solids, *Sci. Rep.* 6 (2016) 1–8, doi:10.1038/srep33451.
- [15] H. Terrones, M. Terrones, E. Hernández, N. Grobert, J.C. Charlier, P.M. Ajayan, New metallic allotropes of planar and tubular carbon, *Phys. Rev. Lett.* 84 (2000) 1716–1719, doi:10.1103/PhysRevLett.84.1716.
- [16] D.H. Robertson, D.W. Brenner, C.T. White, On the way to fullerenes: Molecular dynamics study of the curling and closure of graphitic ribbons, *J. Phys. Chem.* 96 (1992) 6133–6135, doi:10.1021/j100194a011.
- [17] S.T. Skowron, I. V. Lebedeva, A.M. Popov, E. Bichoutskaia, Approaches to modelling irradiation-induced processes in transmission electron microscopy, *Nanoscale.* 5 (2013) 6677–6692, doi:10.1039/c3nr02130k.
- [18] J. Koike, D.F. Pedraza, Dimensional changes in highly oriented pyrolytic graphite due to electron-irradiation, *J. Mater. Res.* 9 (1994) 1899–1907, doi:10.1557/JMR.1994.1899.
- [19] S. Muto, T. Tanabe, Damage process in electron-irradiated graphite studied by transmission electron microscopy. I. high-resolution observation of highly graphitized carbon fibre, *Philos. Mag. A* 76 (1997) 679–690, doi:10.1080/01418619708214029.
- [20] S. Muto, T. Tanabe, Fragmentation of graphite crystals by electron-irradiation at elevated temperatures, *J. Electron Microsc. (Tokyo).* 48 (1999) 519–523, doi:10.1093/oxfordjournals.jmicro.a023710.

- [21] K. Nakai, C. Kinoshita, A. Matsunaga, A study of amorphization and microstructural evolution of graphite under electron or ion irradiation, *Ultramicroscopy*. 39 (1991) 361–368, doi:10.1016/0304-3991(91)90216-S.
- [22] D. Ugarte, Curling and closure of graphitic networks under electron-beam irradiation, *Nature*. 359 (1992) 707–709, doi:10.1038/359707a0.
- [23] A. V. Krashennnikov, K. Nordlund, Ion and electron irradiation-induced effects in nanostructured materials, *J. Appl. Phys.* 107 (2010), doi:10.1063/1.3318261.
- [24] A.P. Burden, J.L. Hutchison, Real-time observation of fullerene generation in a modified electron microscope, *J. Cryst. Growth*. 158 (1996) 185–188, doi:10.1016/0022-0248(95)00547-1.
- [25] F. Banhart, Structural transformations in carbon nanoparticles induced by electron irradiation, *Phys. Solid State*. 44 (2002) 399–404, doi:10.1134/1.1462655.
- [26] K.Y. Wen, T.J. Marrow, B.J. Marsden, The microstructure of nuclear graphite binders, *Carbon N. Y.* 46 (2008) 62–71, doi:10.1016/j.carbon.2007.10.025.
- [27] C. Karthik, J. Kane, D.P. Butt, W.E. Windes, R. Ubic, Microstructural characterization of next generation nuclear graphites, *Microsc. Microanal.* 18 (2012) 272–278, doi:10.1017/S1431927611012360.
- [28] S. Johns, W. Shin, J.J. Kane, W.E. Windes, R. Ubic, C. Karthik, A new oxidation based technique for artifact free TEM specimen preparation of nuclear graphite, *J. Nucl. Mater.* 505 (2018) 62–68, doi:10.1016/j.jnucmat.2018.03.058.
- [29] Zeitler Elmar, Olsen Haakon, Elastic Scattering of Electrons and Positrons by Screened Nuclei , *Zeitschrift Für Naturforsch. A* . 21 (1966) 13-21, doi:10.1515/zna-1966-0901.
- [30] G.H. Kinchin, R.S. Pease, The Displacement of Atoms in Solids by Radiation, *Reports Prog. Phys.* 18 (1955) 1, <http://stacks.iop.org/0034-4885/18/i=1/a=301>.
- [31] M.W. Lucas, E.W.J. Mitchell, The threshold curve for the displacement of atoms in graphite: Experiments on the resistivity changes produced in single crystals by fast electron irradiation at 15°K, *Carbon N. Y.* 1 (1964) 345–352, doi:10.1016/0008-6223(64)90290-8.
- [32] T. Malis, S.C. Cheng, R.F. Egerton, EELS log-ratio technique for specimen-thickness measurement in the TEM, *J. Electron Microsc. Tech.* 8 (1988) 193–200. doi:10.1002/jemt.1060080206.

- [33] M.I. Heggie, Interstitial string model for defective graphites, *Carbon N. Y.* 30 (1992) 71–74, doi:10.1016/0008-6223(92)90108-9.
- [34] R.H. Telling, C.P. Ewels, A.A. El-Barbary, M.I. Heggie, Wigner defects bridge the graphite gap, *Nat. Mater.* 2 (2003) 333–337, doi:10.1038/nmat876.
- [35] T. Trevethan, P. Dyulgerova, C.D. Latham, M.I. Heggie, C.R. Seabourne, A.J. Scott, P.R. Briddon, M.J. Rayson, Extended interplanar linking in graphite formed from vacancy aggregates, *Phys. Rev. Lett.* 111 (2013) 1–5, doi:10.1103/PhysRevLett.111.095501.